AMERICAN SOCIETY FOR MICROBIOLOGY | Journal of Virology

Pathogenesis and Host Response | Full-Length Text

Host factor MxA restricts Dabie bandavirus infection by targeting the viral NP protein to inhibit NP-RdRp interaction and ribonucleoprotein activity

Meng Chang,[1,2] Yuan-Qin Min,[1,3] Zhao Xu,[1,2] Fei Deng,[1,3] Hualin Wang,[1,3] Yun-Jia Ning[1,3,4]

AUTHOR AFFILIATIONS See affiliation list on p. 18.

ABSTRACT Severe fever with thrombocytopenia syndrome (SFTS) is an emerging infectious disease with high case mortality rates, which is caused by Dabie bandavirus (DBV), a novel pathogen also termed as SFTS virus (SFTSV). Currently, no specific therapeutic drugs or vaccines are available for SFTS. Myxovirus resistance protein A (MxA) has been shown to inhibit multiple viral pathogens; however, the role of MxA in DBV infection is unknown. Here, we demonstrated that DBV stimulates MxA expression which, in turn, restricts DBV infection. Mechanistic target analysis revealed that MxA specifically interacts with the viral nucleocapsid protein (NP) in a manner independent of RNA. Minigenome reporter assay showed that in agreement with its targeting of NP, MxA inhibits DBV ribonucleoprotein (RNP) activity. In detail, MxA interacts with the NP N-terminal and disrupts the interaction of NP with the viral RNA-dependent RNA polymerase (RdRp) but not NP multimerization, the critical activities of NP for RNP formation and function. Furthermore, MxA N-terminal domain was identified as the functional domain inhibiting DBV infection, and, consistently, then was shown to interact with NP and obstruct the NP-RdRp interaction. Additionally, threonine 103 within the N-terminal domain is important for MxA inhibition to DBV, and its mutation (T103A) attenuates MxA binding to NP and obstruction of the NP-RdRp interaction. This study uncovers MxA inhibition of DBV with a series of functional and mechanistical analyses, providing insights into the virus–host interactions and probably helping inform the development of antiviral agents in the future.

IMPORTANCE DBV/SFTSV is an emerging high-pathogenic virus. Since its first identification in China in 2009, cases of DBV infection have been reported in many other countries, posing a significant threat to public health. Uncovering the mechanisms of DBV-host interactions is necessary to understand the viral pathogenesis and host response and may advance the development of antiviral therapeutics. Here, we found that host factor MxA whose expression is induced by DBV restricts the virus infection. Mechanistically, MxA specifically interacts with the viral NP and blocks the NP-RdRp interaction, inhibiting the viral RNP activity. Further studies identified the key domain and amino acid residue required for MxA inhibition to DBV. Consistently, they were then shown to be important for MxA targeting of NP and obstruction of the NP-RdRp association. These findings unravel the restrictive role of MxA in DBV infection and the underlying mechanism, expanding our knowledge of the virus-host interactions.

KEYWORDS emerging virus, Dabie bandavirus (DBV), SFTSV, MxA, nucleocapsid protein (NP), ribonucleoprotein (RNP), virus-host interaction, host restriction factor

Severe fever with thrombocytopenia syndrome (SFTS) is an emerging infectious disease characterized by fever, leukopenia, thrombocytopenia, gastrointestinal

Editor Jae U. Jung, Lerner Research Institute, Cleveland Clinic, Cleveland, Ohio, USA

Address correspondence to Hualin Wang, h.wang@wh.iov.cn, or Yun-Jia Ning, nyj@wh.iov.cn.

The authors declare no conflict of interest.

See the funding table on p. 18.

Received 8 October 2023
Accepted 20 November 2023
Published 6 December 2023

symptoms, hemorrhagic complications, and multiple organ failures, associated with high case fatality rates of up to 30% (1, 2). The disease is caused by infection of a novel tick-borne bunyavirus, Dabie bandavirus, also known as SFTS virus (SFTSV), which was first isolated in China in 2009 and then reported in the neighboring countries including South Korea, Japan, and Vietnam (3–6). There are currently no specific antiviral drugs or vaccines available against DBV infection. With its high fatalities and increasing prevalence, the virus has become a new representative high-pathogenic bunyavirus posing a serious threat to public health (7).

Belonging to the genus *Bandavirus*, family *Phenuiviridae*, order *Bunyavirales*, DBV contains a tripartite, single-stranded genome of negative polarity (1, 8, 9). The large (L) segment encodes the RNA-dependent RNA polymerase (RdRp), the medium (M) segment encodes the envelope glycoprotein complex, and the small (S) segment encodes the nucleocapsid protein (NP) and a non-structural protein (NSs) in an ambisense strategy (1). NP encapsidates the viral genome RNA and interacts with RdRP to form the viral ribonucleoprotein (RNP) (10–13). RNPs can act as the viral replication machinery or be packaged into virions as the structural core (10, 11). In the context of the RNP complex, RdRp catalyzes RNA synthesis by interactions with other components of the transcription/replication machinery including template RNA and NP although many molecular details of the transcription/replication processes remain to be determined (8, 10, 11, 13). The viral glycoprotein complex mediates DBV entry into cells and virion packaging (14, 15). Previous studies by us and others have established that NSs can induce the formation of cytoplasmic inclusion body (IB) "jail" by which NSs spatially sequestrates various host proteins to counteract or hijack multiple cellular biological pathways including interferon (IFN) responses and autophagy (16–25). Thus, NSs and NSs-induced IBs play versatile roles at the virus-host interaction interface, contributing to the viral infection and pathogenesis. However, in comparison, host interactions with the viral structural proteins including NP remain largely unclear.

The sophisticated IFN antagonistic strategies evolved by DBV also reflect the critical role of IFN system in host defense against the viral infection. The host antiviral response is initiated from the recognition of virus infection by pattern recognition receptors (PRRs), including retinoic acid-inducible gene I (RIG-I) receptors (especially RIG-I) and several toll-like receptors (19, 26). The PRR signaling then triggers the expression of type I and III IFNs and proinflammatory cytokines. Secreted IFNs further stimulate the expression of hundreds of IFN-stimulated genes (ISGs) through the Janus kinase-signal transducer and activator of transcription (JAK-STAT) signaling, establishing an antiviral state for host cells (27). In addition, in the early stage of infection, viruses may also directly cause the expression of some ISGs, which, thus, are also named virus-stimulated genes (VSGs), through the PRR signaling. The mechanisms of the interactions between specific ISGs or VSGs and DBV have yet to be studied in detail. Myxovirus resistance A (MxA), a representative ISG, is found in approximately all vertebrates and has antiviral properties against multiple RNA and DNA viruses (28–34). Nevertheless, the precise molecular mechanisms of MxA inhibiting these viruses are still not clearly clarified. There are also no studies on whether and how MxA may regulate the replication of DBV.

In this study, we found that DBV can stimulate MxA expression from the early stage of infection and, in turn, MxA exerts a significant suppressive effect against the viral infection. Then, we investigated and mechanistically characterized MxA inhibition of DBV. MxA specifically targets the viral NP (but not the other proteins) in an RNA-independent manner and, therefore, impairs the interaction of NP with RdRp, blocking the RNP activity and inhibiting the viral replication. Furthermore, the N-terminal region of NP is required for MxA targeting, and in turn, the N-terminal of MxA was shown to be the NP-binding domain. Consistently, the MxA N-terminal was further demonstrated to be the functional domain that inhibited NP-RdRp interaction and the virus infection even when expressed alone. Additionally, a residue (Thr 103) within the MxA N-terminal was identified as a critical amino acid site for the targeting of NP and, hence, the inhibition of

NP-RdRp interaction and DBV infection. These findings provide new mechanistic insights into DBV-host interactions and the antiviral activities of MxA.

RESULTS

DBV stimulates MxA expression which, in turn, restricts the viral infection

To elucidate the potential interplays of MxA with DBV, we first monitored MxA expression upon DBV infection. DBV-permissive human cells including A549, THP-1, and HEK293 were infected with DBV and subjected to qPCR analyses of MxA mRNA levels at the indicated time points post infection (p.i.). As shown in Fig. 1A through C, MxA expression was, indeed, induced by DBV infection in all the cells analyzed albeit to different extents. Moreover, notable upregulation of MxA could be detected (especially in A549 cells), or even peaked (in THP-1 cells), at the early phase of infection (6 h p.i.), suggesting that MxA is likely not only an ISG but also a possible VSG induced by DBV.

We then analyzed the potential influence of up-regulated MxA expression on DBV infection. HEK293 cells transfected with a MxA expression plasmid were infected with DBV, followed by analyses of the viral protein expression, RNA accumulation, and progeny propagation at different time points. As presented in Fig. 1D, DBV protein production was evidently reduced in cells transfected with the MxA expression plasmid, compared to the control. Moreover, qPCR analyses further showed that MxA overexpression could significantly decrease the viral RNA levels (Fig. 1E through G). Consistently, titers of the progeny DBV released to culture medium supernatants were significantly decreased by MxA overexpression, compared with the control (Fig. 1H). These findings suggest that MxA likely has a notable inhibitory activity against DBV infection.

Effects of MxA knockout (KO) by CRISPR-Cas9 gene editing on DBV infection

To further confirm the anti-DBV role of MxA, we generated MxA-KO HEK293 cells by the CRSPR-Cas9 gene editing system. After validation by sequencing and Western blotting (Fig. 2A and B), the MxA-KO cells together with the wild-type control were used for comparison of DBV infection. In agreement with the results obtained by overexpression, MxA KO results in an increase of the levels of viral proteins and RNAs (Fig. 2C and D). Consistently, a significant increase of the progeny propagation was also observed (Fig. 2E). Together, these data confirm that MxA is a cellular antiviral factor against DBV.

MxA specifically targets the NP protein of DBV

To unravel the molecular mechanism underlying MxA restriction to DBV, we first identified the potential viral protein(s) targeted by MxA. As shown in the protein interaction analyses by S-pulldown assay, DBV NP, but not the other viral proteins, was specifically co-precipitated by MxA (Fig. 3A), indicating a specific targeting of the viral NP by MxA. Furthermore, a reciprocal pulldown assay with S-tagged NP as the bait confirmed the interaction of MxA with NP (Fig. 3B). NP has RNA-binding potential. To explore whether RNA is involved in the interaction between MxA and NP, pulldown assays were further conducted with cell lysate samples that were similarly prepared as in Fig. 3B but then subjected to excessive nuclease treatment or left untreated as control (12). Compared to the control, the coprecipitation of MxA and NP was not noticeably damaged by nuclease treatment (Fig. 3C), indicating that the MxA-NP interaction likely is not mediated by RNA. Then, the cellular distribution of MxA and DBV NP was analyzed by immunofluorescence assay (IFA). Under confocal microscopy, colocalization of MxA with DBV NP was observed in cells co-transfected with the MxA and NP expression plasmids (Fig. 3D), in line with the protein interaction. Moreover, MxA colocalization with NP could also be seen in the context of DBV infection (Fig. 3E). Together, these results suggest the targeting of DBV NP by MxA.

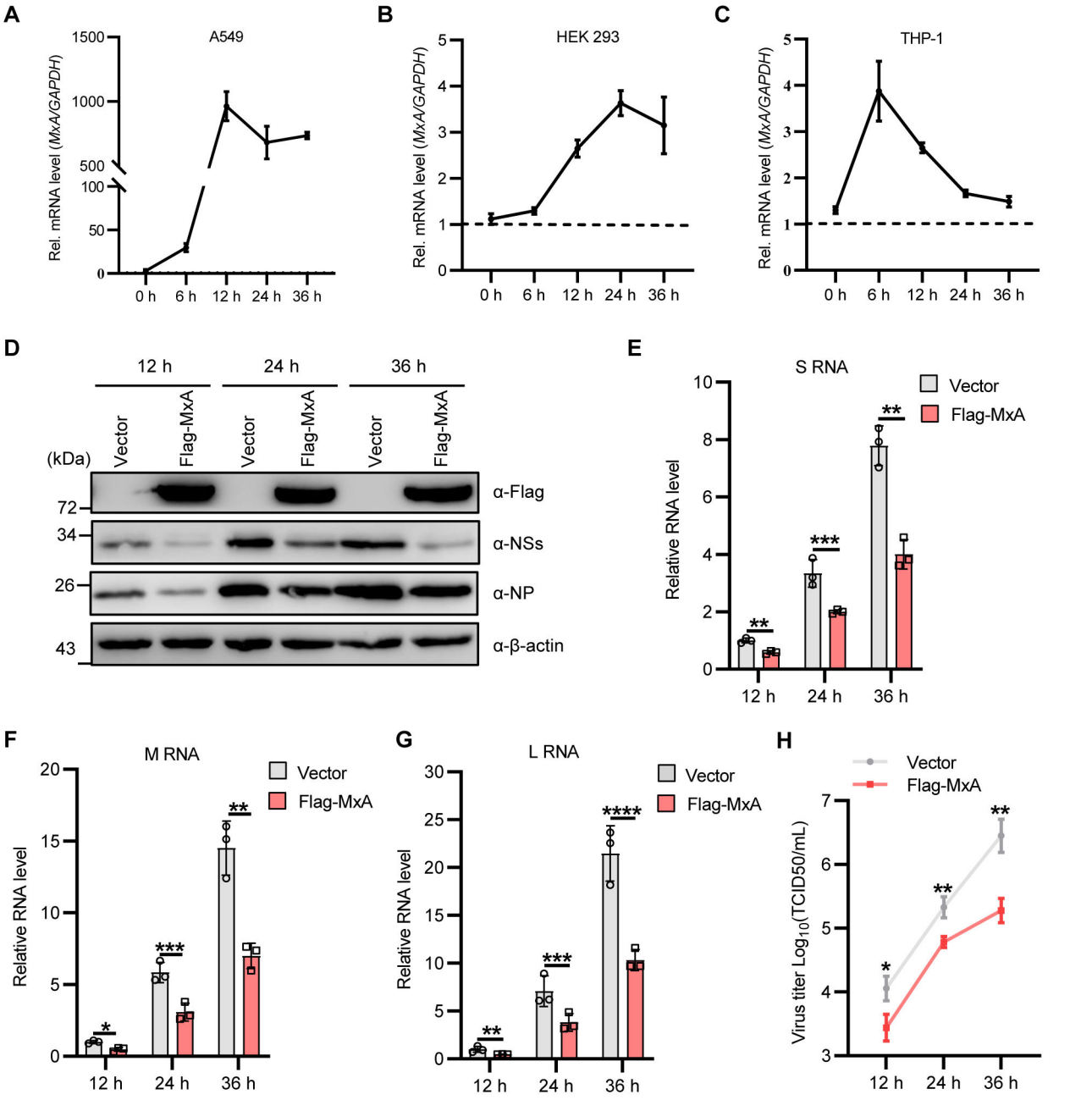

FIG 1 DBV infection stimulates MxA expression that, in turn, inhibits DBV infection. (A–C) DBV infection stimulates MxA expression. A549 (A), HEK293 (B), or THP1 (C) cells were, respectively, infected with DBV at a multiplicity of infection (MOI) of 5 and then harvested at the indicated time points for detection of the dynamic changes of MxA mRNA levels by qPCR. (D–H) MxA overexpression restricts DBV infection. HEK293 cells were transfected with the Flag-MxA expression plasmid or control vector, followed by DBV (0.1 MOI) infection. At the indicated time points post infection (p.i.), cells were then lysed for detection of the viral proteins by Western blot (WB) with the indicated antibodies (D) or for quantitative PCR (qPCR) analyses of viral S, M, or RNA levels, respectively (E–G). The propagation of progeny viruses released into the culture medium was also monitored by titration with the TCID50 method (H). Data show means ± SD, $n \geq 3$. *$P < 0.05$; **$P < 0.01$; ***$P < 0.005$; ****$P < 0.001$.

MxA inhibits DBV RNP activity

NP acts as the major protein component and drives the formation of the viral RNP which is the transcription/replication machinery and structural core of virions (8, 10, 11, 13, 35). NP-directed RNP formation and RdRp-catalyzed RNA synthesis in the RNP context are central events of DBV infection (10, 11). Considering MxA targeting of NP and inhibition of DBV infection, we hypothesized that MxA may affect the viral RNP activity. Therefore,

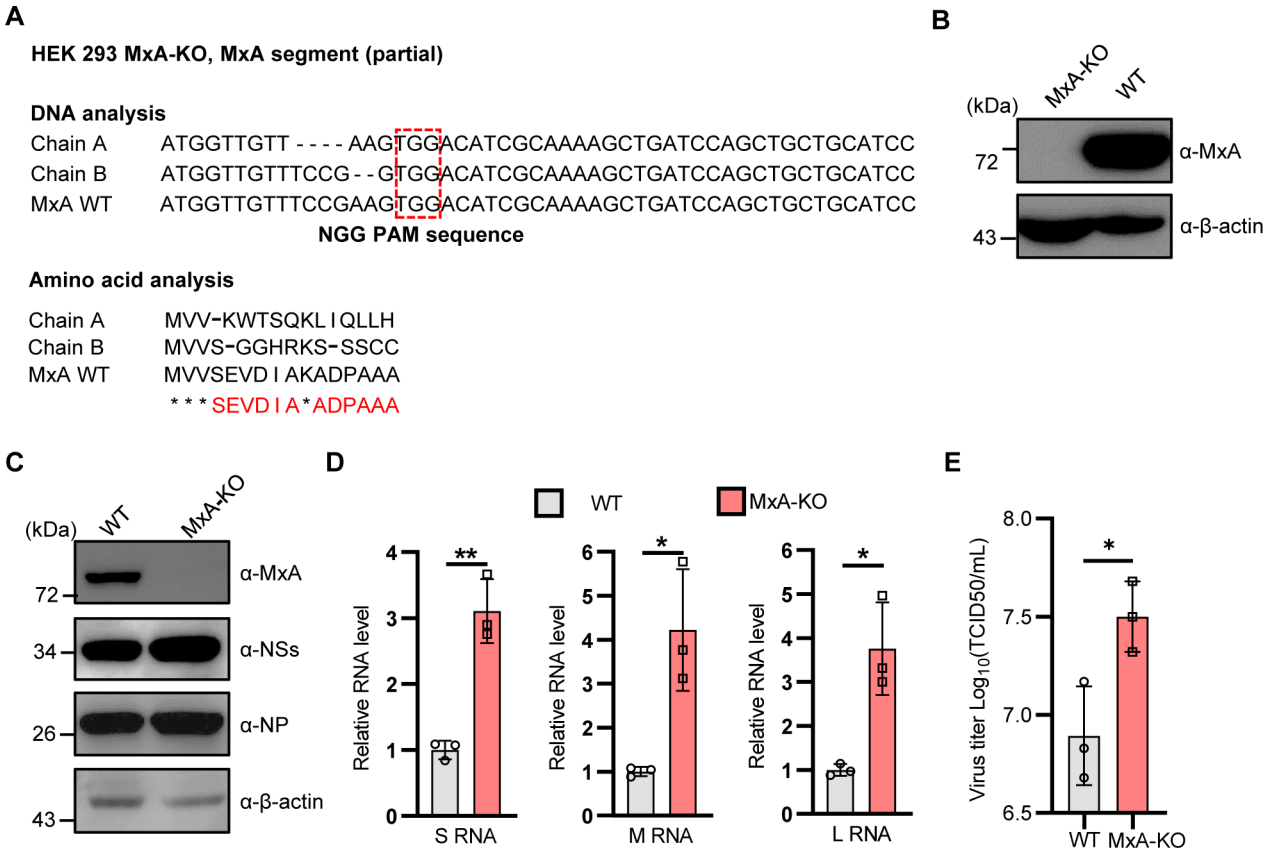

FIG 2 Effects of MxA Knockout by CRISPR-Cas9 on DBV infection. (A, B) Generation of the MxA-KO cell clone by CRISPR/Cas9-mediated gene editing. Validation of the MxA-KO cells by DNA sequencing is shown in (A). Additionally, the cells were also confirmed by Western blotting (B). As the endogenous protein level of MxA was relatively low, the MxA-KO and wild-type cells were first infected with DBV for 24 h to boost the MxA protein expression and then analyzed by Western blot (B). (C–E) MxA-KO enhances DBV infection. MxA-KO or control HEK293 cells were infected with DBV (MOI = 0.1). At 36 h p.i., cells were delivered to analyses of viral protein (C) and RNA levels (D). The culture medium supernatants were also harvested to detect progeny propagation by the TCID50 method (E). Data show means ± SD, $n = 3$. $^{*}P < 0.05$; $^{***}P < 0.001$.

we next tested the hypothesis by a minigenome system that reconstitutes the viral RNP complex and can be exploited as a reporter of the RNP activity (36). The DBV NP and RdRp expression plasmids and a minigenome reporter plasmid (MUTR-EGFP) (36) were co-transfected into cells, together with the MxA expression plasmid or control vector. As shown in Fig. 4A and B, EGFP reporter expression was successfully driven by the RNP reconstitution in the minigenome system (middle groups of Fig. 4A and B). However, the EGFP reporter was significantly repressed in cells transfected with the MxA expression plasmid (Fig. 4A and B), suggesting MxA inhibition of the RNP activity. Moreover, similar results were obtained by using another minigenome system based on dual luciferase reporters (36) (Fig. 4C), further confirming the strong inhibition of SFTSV RNP by MxA. As controls, we also analyzed the possible effects of MxA on the virus entry to host cells including the cell surface binding and internalization processes using methods previously reported (37, 38). In contrast, MxA expression did not exhibit any significant influence on the virus entry processes, whether the virus binding (Fig. 4D) or the internalization (Fig. 4E). Collectively, these results indicate that by interacting with NP, MxA specifically interferes with the RNP activity.

MxA binds to the N-terminal region of NP

To further reveal the MxA-NP interaction mechanism, we analyzed the key regions of NP to which MxA targets. A series of NP mutants constructed based on the protein structure (12, 35) were used for interaction domain mapping by S-pulldown (Fig. 5A and B).

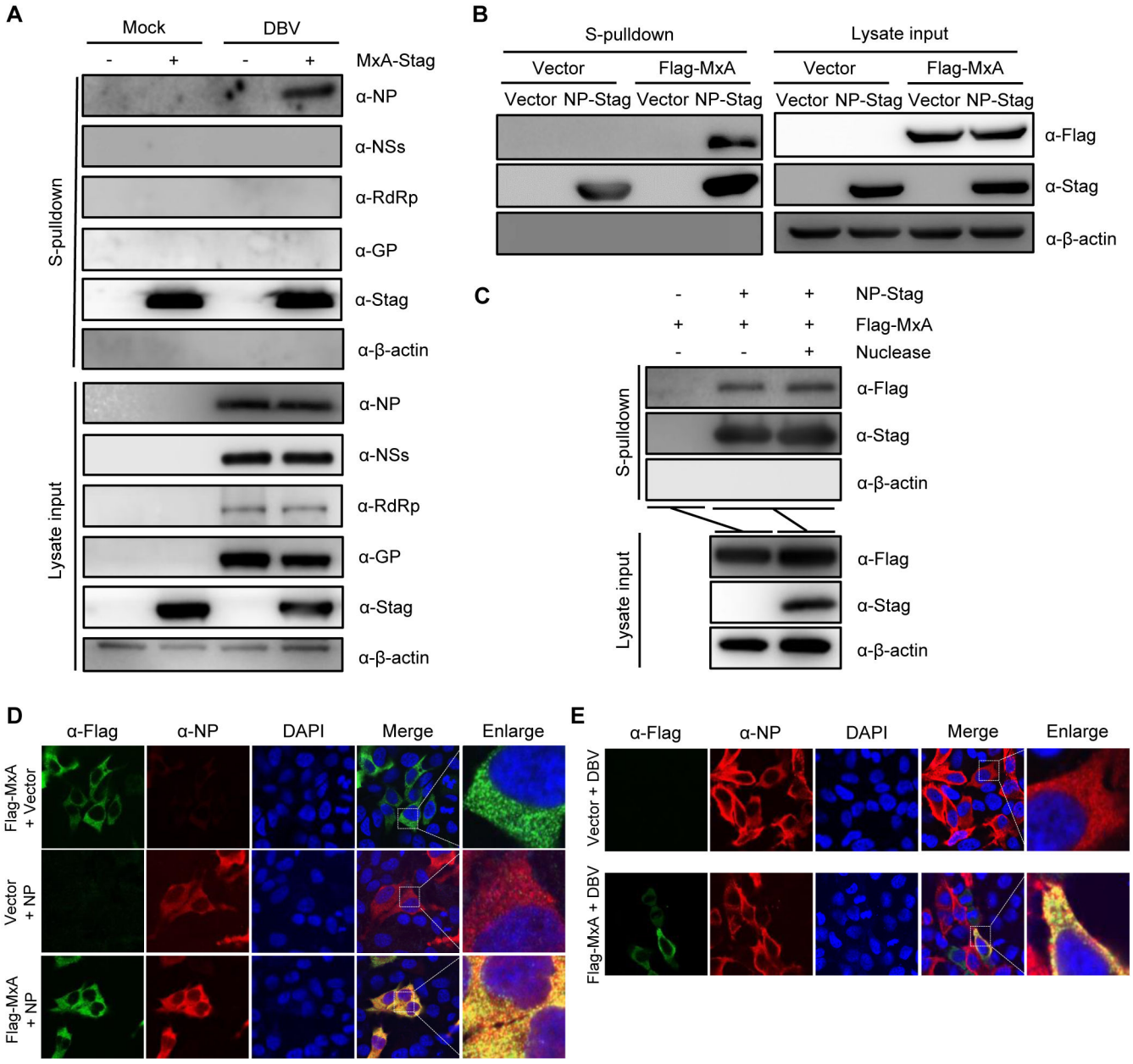

FIG 3 DBV NP is the target of MxA. (A) MxA specifically interacts with the NP protein of DBV. HEK293T cells were transfected with the control vector or the plasmid expressing S-tagged MxA (MxA-Stag), followed by DBV infection at 6 h post-transfection. At 48 h p.i., cells were subjected to S-pulldown assay, followed by WB detection of the input and pulldown products with the specific antibodies. β-Actin was used as the loading and negative interaction control. GP analysis was performed with specific rabbit antiserum against the representative Gn subunit. (B) Reciprocal pulldown assay with NP as the bait. HEK293T cells were co-transfected with the plasmid encoding S-tagged NP (NP-Stag) and the Flag-MxA expression plasmid, or the control vectors. At 48 h post-transfection, cells were subjected to S-pulldown assay, followed by WB detection. (C) The MxA-NP interaction is independent on RNA. HEK293T cells were co-transfected with the NP-Stag and Flag-MxA encoding plasmids or the control vector. At 48 h post-transfection, cells lysate supernatants were treated with UltraNuclease or left untreated as indicated, followed by S-pulldown and WB analysis of the protein interactions. (D) HeLa cells were transfected with the Flag-MxA and NP expression plasmids or the control vectors. At 24 h post-transfection, the expression and localization of MxA (green) and NP (red) were visualized by confocal microscopy, following immunofluorescence assay (IFA) by using the indicated antibodies. (E) HeLa cells transfected with the Flag-MxA expression plasmid or the control vector were infected with DBV at 6 h post-transfection. At 24 h p.i., the expression and localization of MxA (green) and NP (red) were visualized by IFA and confocal microscopy. Nuclei stained with Hochest33258 are shown in blue.

Consistent with the previous observations (12), truncation of NP resulted in a reduction of the protein expression levels to different extents (Fig. 5C). Despite that, S-pulldown

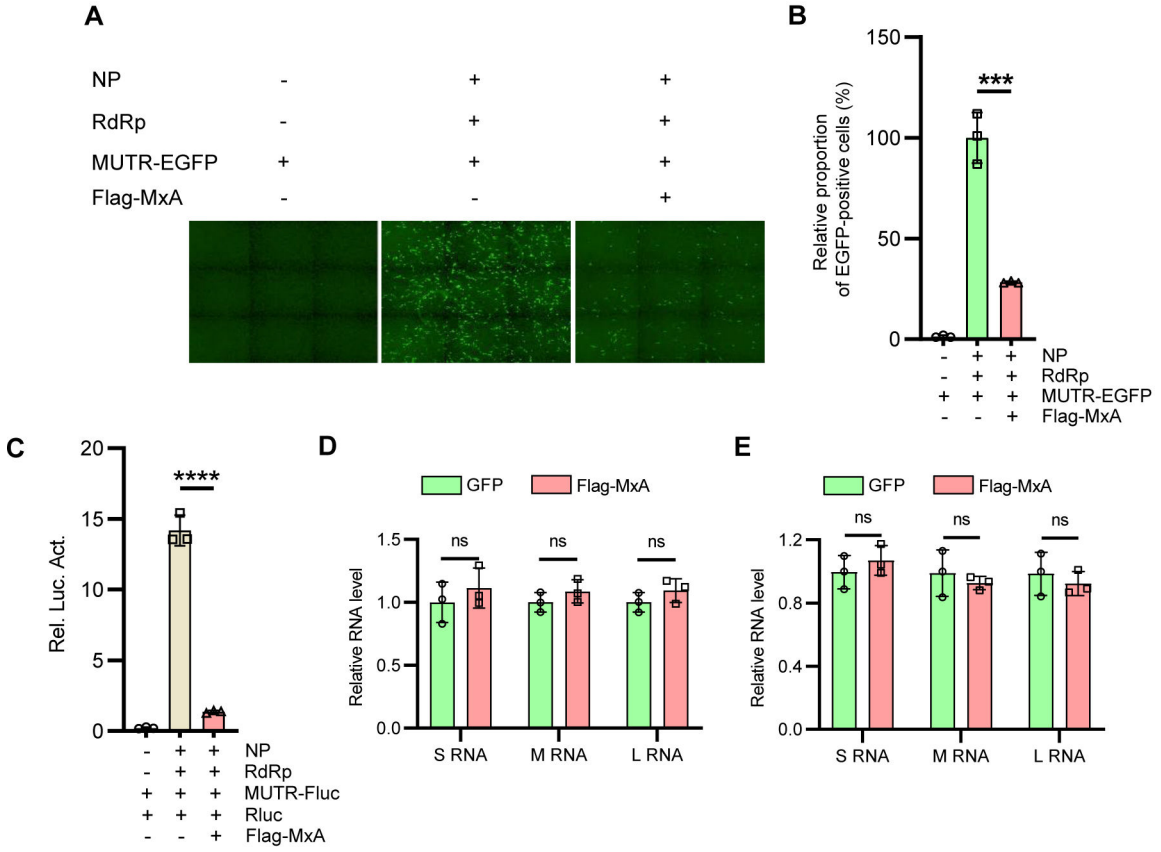

FIG 4 MxA inhibits DBV RNP activity. (A and B) MxA inhibits the activity of DBV minigenome RNP reporter. DBV NP and RdRp expression plasmids, and a minigenome reporter plasmid encoding a viral M genome analog containing EGFP reporter sequence flanked by M untranslated regions (UTRs) were co-transfected into BHK21 cells, together with the MxA expression plasmid or control vector. At 48 hours post-transfection, cells were fixed and stained with Hoechst 33258, followed by high-content imaging and counting of EGFP-positive cells. Nine fields per well were successively scanned as shown in (A). Statistical analyses from three independent biological replicates were presented in (B). (C) A minigenome RNP reconstitution assay based on dual luciferase reporters corroborated the inhibition of the RNP activity by MxA. The firefly luciferase (Fluc)-based minigenome transcription plasmid (MUTR-Fluc) and an internal control pRL-TK expressing *Renilla* luciferase (Rluc) were used to replace the MUTR-EGFP transcription plasmid for co-transfection. Relative luciferase activities (Rel. Luc. Act.) were calculated and shown, following dual luciferase reporter detection. (D and E) The effects of MxA on virus binding and internalization. HEK293T cells were transfected with the MxA or EGFP (control) expression plasmids. At 24 h post-transfection, cells were incubated with DBV, followed by qPCR analyses of the bound (D) or internalized (E) viruses as described in Materials and Methods. Data are presented as means ± SD, $n = 3$. ***$P < 0.001$; ****$P < 0.0001$; ns, no significance.

assays could still reveal that the truncated mutant with the C-lobe deleted, here named NP(1-111), retains evident interaction with MxA, whereas the mutant consisting of 35–246 amino acids, NP(35-246), cannot be noticeably coprecipitated with MxA (Fig. 5C). The results suggest that the N-terminal region is likely the main binding domain for MxA and, based on the coprecipitation results with NP(1-111) and NP(35-246), the N-arm may be a needed motif. To further determine the role of N-arm in the protein interaction, we conducted an additional EGFP nano-trap analysis (12, 39, 40) with cells co-transfected with the MxA expression plasmid and the plasmid encoding EGFP-tagged N-arm and full-length NP or control vectors. As shown in Fig. 5D, we found that MxA could be coprecipitated with full-length NP but not with the N-arm domain, indicating that N-arm is not sufficient for MxA targeting of NP. Together, these analyses indicate that the N-terminal region of NP is likely the MxA-binding domain, and both the N-arm and N-lobe in this region seem to be required.

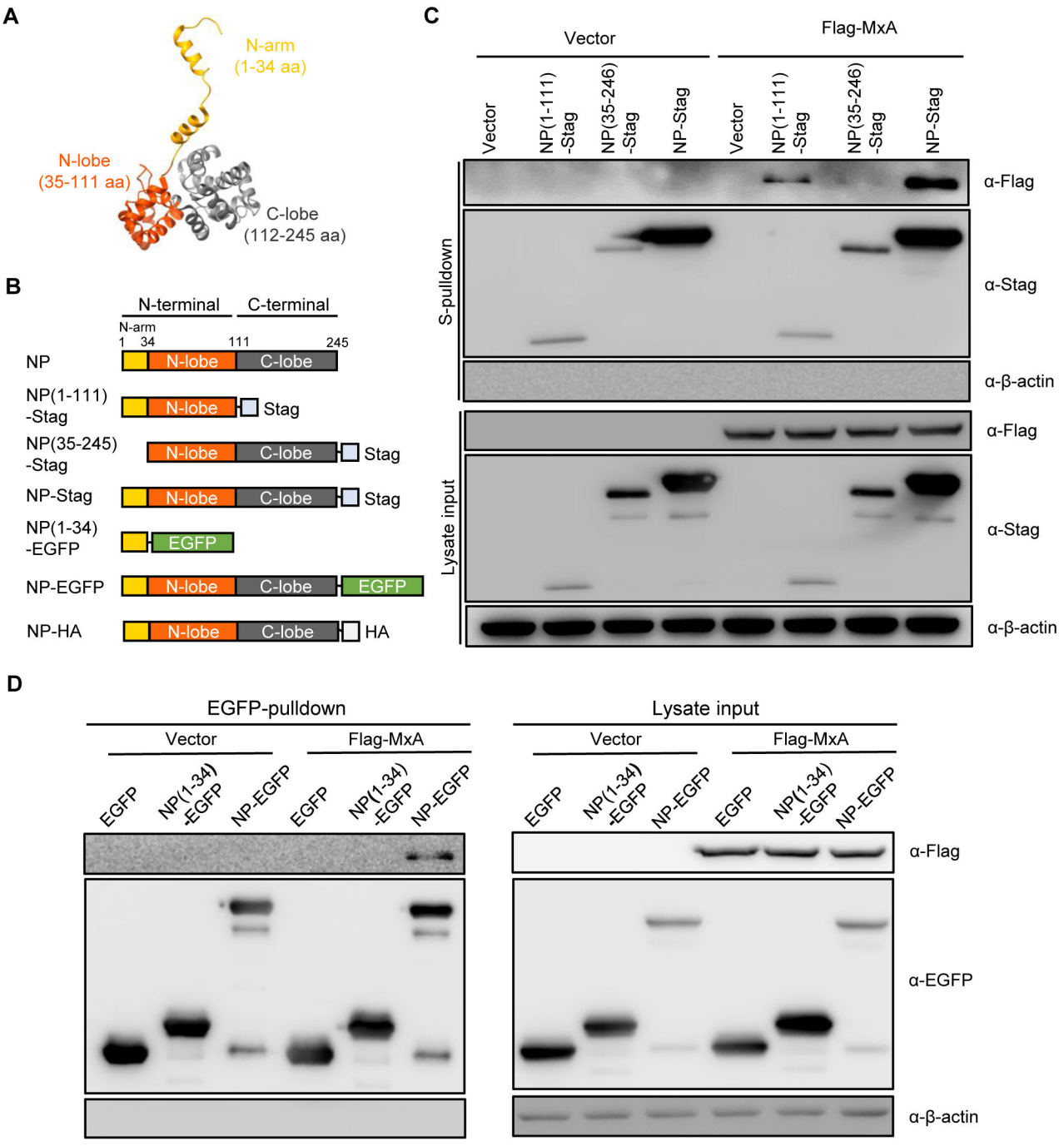

FIG 5 MxA binds to the N-terminal region of NP. (A) The structure of DBV NP (PDB: 4J4R). The N-terminal region of DBV NP consists of an N-arm and an N-lobe, while the C-terminal folds into a C-lobe. (B) Schematic diagram of NP truncations used in this study. (C) HEK293T cells were co-transfected with the plasmids expressing the indicated S-tagged NP truncated mutants and Flag-MxA or the control vectors. At 48 h post-transfection, protein interactions were analyzed by S-pulldown and WB. (D) HEK293T cells were transfected with the plasmids encoding EGFP or EGFP-tagged NP or NP-arm (1–34 aa). At 48 h post-transfection, cells were subjected to EGFP-nanotrap and WB analysis of the lysate input and pulldown products.

MxA blocks the NP-RdRp interaction but not NP polymerization

Interactions between the components of the RNP complex including NP multimerization (NP-NP interaction) and NP-RdRp interaction are important for RNP formation and function (8, 10–12, 35, 41). To further mechanistically address MxA inhibition of RNP by targeting NP, we first examined the effect of MxA on NP polymerization by chemical

cross-linking assays (12, 42). However, compared to the control group, no noticeable effect of MxA on NP polymerization was observed (Fig. 6A). Then, the influence of MxA on the interaction between NP and RdRp was also investigated. Interestingly, as shown in Fig. 6B, MxA indeed, attenuated the NP-RdRp interaction in a dose-dependent manner. Together, these data suggest that MxA binds to NP and thereby obstructs the NP-RdRp interaction, inhibiting the RNP activity.

Mapping of MxA domain(s) required for the targeting of NP/RNP and inhibition of DBV infection

To find more mechanistical details of MxA targeting of DBV NP, we also analyzed the domain(s) of MxA important for its interaction with NP. Based on the structure and linear organization of MxA, we truncated the protein into N-terminal and C-terminal regions (43). A Leu-rich loop (referred to as Loop 4) located in the C-terminal region has been reported as an important motif required for MxA anti-orthomyxovirus activity (44) and, thus, was also analyzed in our study. First, HEK293T cells were co-transfected with the NP-Stag expression plasmid and the plasmid encoding the N- or C-terminally truncated or loop-deleted mutants, or control vectors, followed by protein interaction analysis. As shown in the following S-pulldown assays, except for the N-terminal deleting mutant (MxAdelN), the other mutants with the C-terminal or loop removed (named MxAdelC or MxAdelL, respectively) and wild-type MxA could be coprecipitated by DBV NP (Fig. 7C). This suggests that the N-terminal of MxA likely plays the role as the binding domain to DBV NP, whereas the C-terminal and loop are dispensable for the interaction. Interestingly, in agreement with the abilities to target NP, the N-terminal domain alone (MxAdelC) retained the anti-DBV activity, while its deletion (MxAdelN), but not the deletion of the loop (MxAdelL), disrupted the capacity to inhibit DBV infection, as shown in Western-blot analyses of the viral protein expression (Fig. 7D). Moreover, consistent results were obtained when the viral RNA levels were analyzed by qPCR (Fig. 7E). Furthermore, additional protein interaction analyses showed that MxA N-terminal

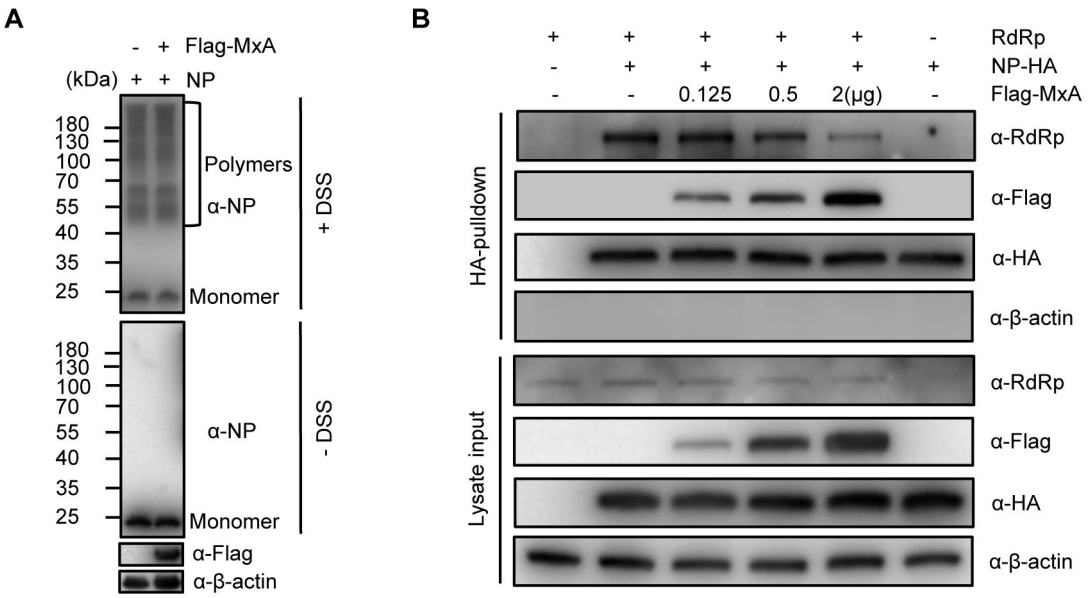

FIG 6 MxA disturbs the interaction of NP with RdRp but not the NP polymerization. (A) The effect of MxA on NP polymerization. HEK293 cells were transfected with the expression plasmid for DBV NP, together with the Flag-MxA expression plasmid or control vector. At 48 h post-transfection, cells were subjected to cross-linking with disuccinimidyl suberate (DSS) as described in Materials and Methods, followed by SDS-PAGE and WB analysis of NP monomer and fixed oligomeric forms. (B) MxA inhibits the NP-RdRp interaction. Cells were co-transfected with the NP-HA and RdRp expression plasmids, together with indicated amounts of the Flag-MxA expression plasmid. At 48 h post-transfection, cells were lysed and subjected to HA-pulldown and WB by using the indicated antibodies.

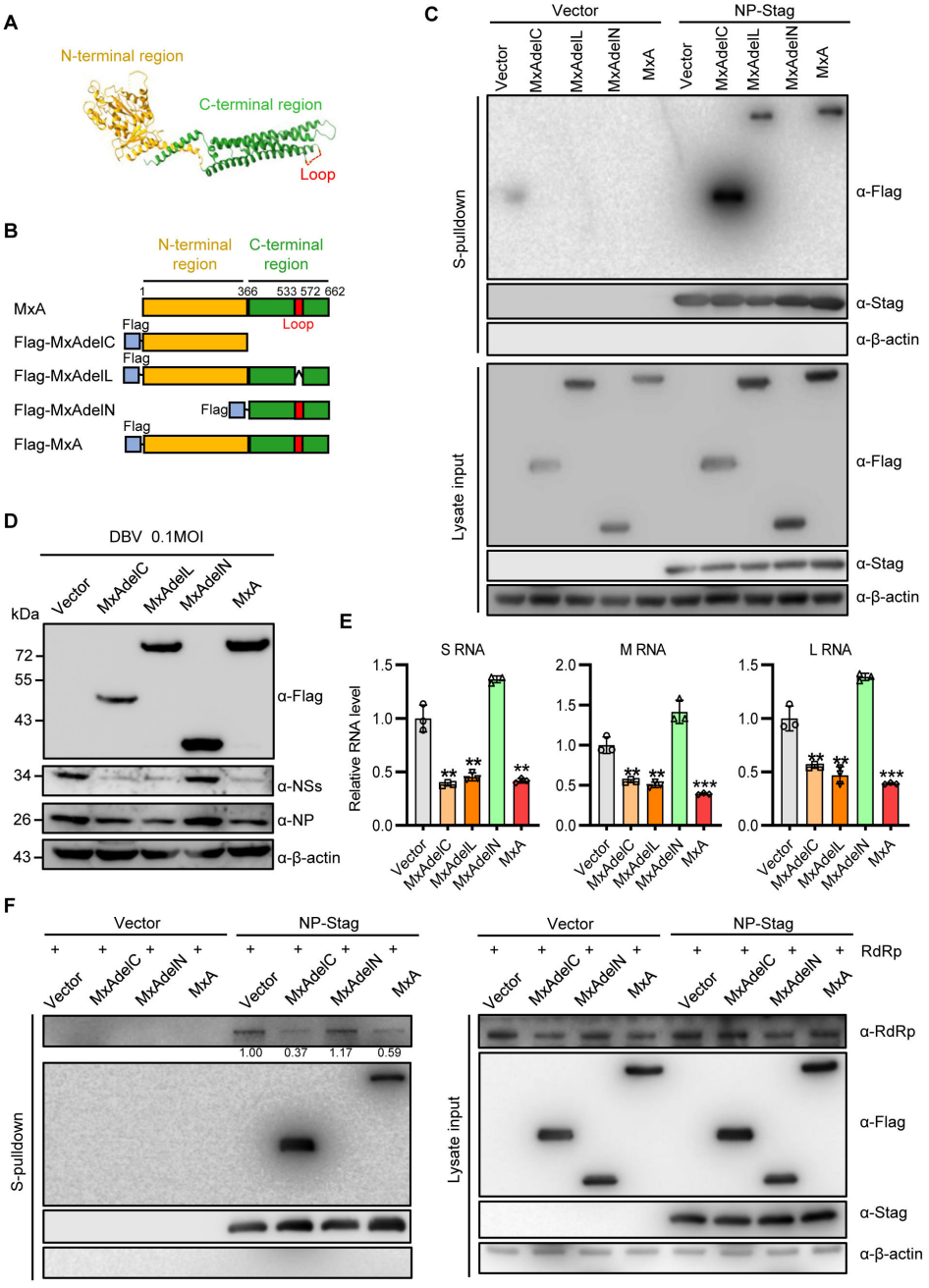

FIG 7 Mapping of MxA domain(s) required for the targeting of NP/RNP and inhibition of DBV infection. (A) Ribbon-type representation of MxA structure (PDB: 3SZR). The N-terminal region (head) is indicated in gold, the C-terminal (stem) in dark green, and the Loop 4 marked by dotted line in red. (B) Schematic diagram of MxA truncations used below. (C) MxA N-terminal is required for targeting of NP by acting as the NP-binding domain. HEK293T cells were co-transfected with the NP-Stag expression plasmid and the plasmids expressing Flag-tagged MxA or truncated mutants, or the control vectors for 48 h, and then subjected to S-pulldown and WB analyses. (D, E) The N-terminal is MxA functional domain inhibiting DBV. Cells transfected with the full-length or truncated MxA expression plasmids or control vector were infected with DBV (0.1 MOI) at 24 h post-transfection. At 24 h p.i., viral protein and RNA levels were analyzed by WB (D) and qPCR (E), respectively. (F) The functional N-terminal is sufficient to inhibit NP-RdRp interaction, while its deletion disrupts the ability. Cells were co-transfected with the RdRp and NP-HA expression plasmids, together with the plasmids encoding MxA or its truncated mutants and then subjected to pulldown and WB analysis. Band intensities of co-precipitated RdRp were quantified with ImageJ software and normalized to the control group (vector). Data are presented as means ± SD, $n = 3$. $^{**}P < 0.01$; $^{***}P < 0.001$.

(MxAdelC), indeed, blocked the NP-RdRp interaction; however, its deletion abolished the ability (Fig. 7F). These data are consistent with and provide further supportive evidence for the mechanism of full-length MxA action revealed above, establishing that the N-terminal is the functional domain for MxA targeting of NP, blockade of NP-RdRp interaction, and inhibition of DBV infection.

Thr 103 of the functional N-terminal region is an important amino acid residue for MxA anti-DBV function

Following identification of the functional N-terminal, we tried to identify a critical amino acid site involved in MxA anti-DBV activity. We considered that it would not only provide additional insight into MxA targeting of DBV NP but also help us further verify the mechanism of MxA action. Based on the literature, a hydrophilic amino acid, threonine 103 (T103) of the N-terminal domain, has been proved a key residue in MxA antiviral activities against multiple viruses such as influenza A virus (IAV) and Thogoto virus (THOV) (45–47). However, it seems not to be required for MxA inhibition to hepatitis B virus (HBV) (48). We, thus, evaluated the effect of the Thr103 on MxA anti-DBV activity. As seen in Fig. 8A and B, replacement of T103 by alanine (T103A mutation), indeed, impaired MxA inhibition to DBV infection. Consistently, we observed that the interaction of MxA with NP is also obviously attenuated by the mutation of Thr103 (Fig. 8C). Interestingly, we further demonstrated that the T103A mutant exhibited a weakened ability to obstruct the NP-RdRp interaction, along with the decreased interaction with NP (Fig. 8D). These consistent results indicate that Thr 103 is a key residue for MxA inhibition of DBV, as it is likely required for the optimal activity to target NP and block the NP-RdRp interaction, validating the mechanical mode of MxA anti-DBV action again. Altogether, these data provide further detailed insights into MxA targeting of NP and inhibition of DBV infection.

DISCUSSION

Given the high fatalities, multiple transmission modes (tick bites and animal/human-to-human contacts), increasing prevalence and lacking of antivirals and vaccines, DBV has been considered a priority pathogen candidate requiring greater research and development efforts (7, 49). However, limited knowledge on the mechanisms of the viral infection and pathogenesis impedes the development of treatment and prevention strategies. Thus, there is an urgent need for the better understanding of the virus-host interactions to advance not only the elucidation of viral infection and host response mechanisms but also the antiviral research. In this study, we found that DBV can induce MxA expression from the early stage of infection. In turn, MxA significantly restricts DBV infection. Then, DBV NP was identified as the specific target that is bound by MxA in RNA-independent manner. Further, by its N-terminal domain, MxA can target the N-terminal region of NP and block the NP-RdRp interaction, inhibiting the RNP activity and, hence, DBV infection (summarized in a proposed model in Fig. 9). These findings provide new insights into the virus-host interplays (particularly the host antiviral responses) and the MxA functioning mechanism as a host restriction factor.

DBV RNPs are the viral RNA synthesis machinery catalyzing transcription and replication processes via complex interactions of the RNP molecular elements including not only viral nucleic acids but also the proteins, NP and RdRp, although the precise interaction mechanisms underlying RNP activities remain to be fully determined (10, 11, 35, 41). Moreover, RNPs containing viral genomic RNAs (vRNPs) also can be packaged into progeny virion as the structural core (50). Therefore, viral RNPs and their delicate activities could be targets for host antiviral defense and for therapeutic design. In a previous study, we have found that another ISG induced by DBV infection, MOV10 also can target DBV RNP by interacting with NP (12). MOV10 specifically binds to the short N-arm of NP that, moreover, is sufficient for MOV10 targeting. In comparison, the whole N-terminal region of NP is likely required for MxA interaction. Furthermore, MOV10 can impair not only NP interaction with RdRp but also NP multimerization, whereas MxA here

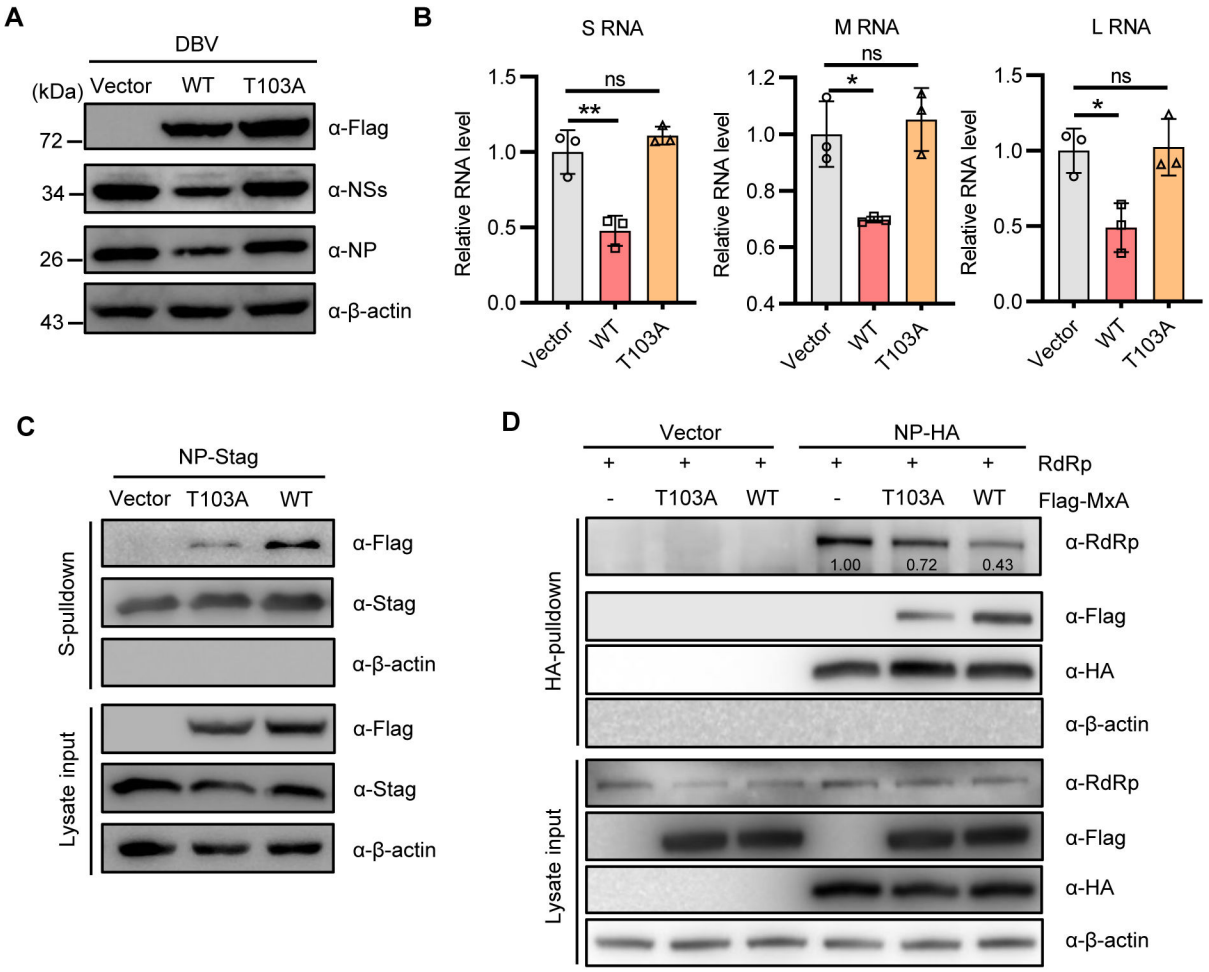

FIG 8 Thr 103 of MxA is an important residue for efficient targeting of NP and optimal inhibitory activities against the NP-RdRp interaction and DBV infection. (A, B) Thr 103 is required for optimal anti-DBV activity of MxA. HEK293 cells were transfected with the plasmids encoding Flag-tagged wild-type MxA (WT) or T103A mutant, or the control vector. At 24 h post-transfection, cells were infected with DBV (0.1 MOI) for 24 h, followed by WB (A) and qPCR analyses (B). Data in (B) show means ± SD, $n = 3$. *$P < 0.05$; **$P < 0.01$; ns, non-significant. (C) Thr 103 mutation reduces MxA interaction with NP. Cells were co-transfected with the NP-Stag expression plasmids and the plasmids expressing Flag-tagged wild-type MxA or MxA T103A mutant, or the control vector. At 48 h post-transfection, protein interactions were analyzed by pulldown assays. (D) Thr 103 mutation of MxA weakens its ability to inhibit NP-RdRp interaction. Cells were co-transfected with the plasmids expressing RdRp and NP-HA or the control vector, together with the plasmid encoding Flag-tagged wildtype MxA or T103A mutant, or the control vector. At 48 h post-transfection, cells were subjected to pulldown and WB analysis of protein interactions. Relative band intensities of co-precipitated RdRp were calculated as in Fig. 7F.

was shown to specifically block the NP-RdRp interaction (but not NP multimerization), reflecting differences in the mechanism of action. These findings support the possibility that DBV RNP is likely a vulnerable target in host antiviral response and the detailed mechanisms employed by host antiviral proteins could be diverse. Additionally, it will be interesting to explore whether and how these host restriction factors can suppress the virus infection synergistically, contributing to the host antiviral defense together.

MxA has inhibitory activities against a variety of viruses, attracting a lot of research interests previously (34, 46, 51–55). However, the exact mechanisms underlying MxA antiviral function against these viruses remain misunderstood. The best-known case is its significant restriction of IAV infection and trans-species transmission into human population. Although the precise molecular mechanism is still elusive, it has been proposed that MxA may bind to IAV vRNP by targeting the viral NP to block vRNP nuclear import essential for IAV replication. A similar action of MxA was also proposed in its inhibition against Thogoto virus, another orthomyxovirus that replicates in the

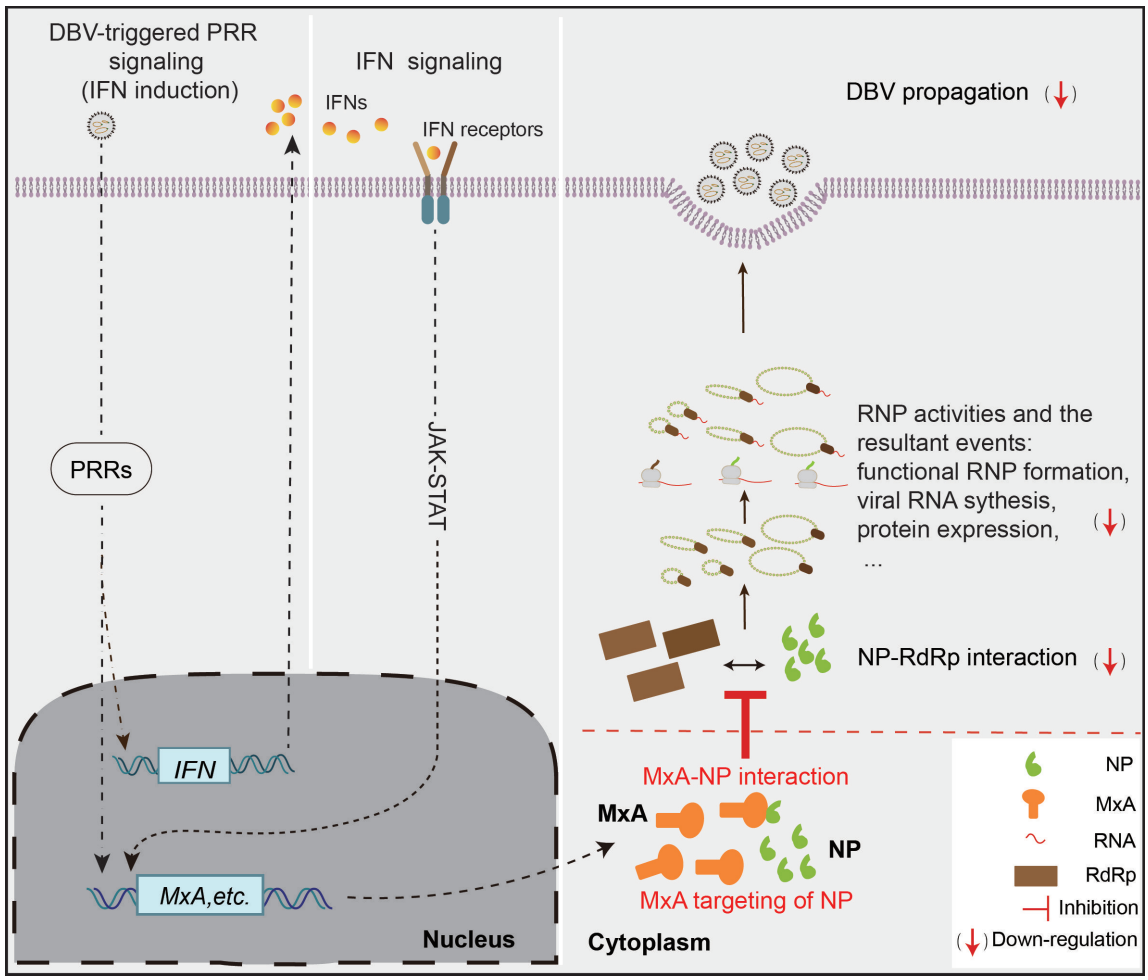

FIG 9 Proposed model for restriction of DBV by host factor MxA. DBV infection can stimulate MxA expression likely by both the later IFN signaling and the earlier PRR signaling triggered by recognition of the virus infection. MxA, in turn, targets the NP protein of DBV by binding between their N-terminal domains and blocks the NP-RdRp interaction and the viral RNP activity, thus restricting DBV infection. See also text for details.

nucleus. These studies suggest a possibly general antiviral mechanism by interfering with vRNP import to the nucleus. However, it could be different for other viruses, like DBV, that replicate exclusively in cytoplasm. Here, our study shows that MxA can bind to the N-terminal of DBV NP and disrupt NP-RdRp interaction to inhibit the viral RNP by its N-terminal region, presenting a new mode of action for MxA antiviral function. Based on the crystal structures, MxA is mainly comprised of an N-terminal globular GTPase-containing head (G-domain) corresponding to the majority of the N-terminal region in linear organization and a C-terminal helical stalk belonging to the C-terminal region. The G-domain head and the stalk are connected by a hinge-like bundle-signaling element (BSE) that is consisting of three α-helixes separately locating in the N- and C-terminal regions. The stalk and BSE are required for MxA oligomerization and, hence, oligomerization-dependent GTP hydrolysis. These intrinsic elements of MxA including the G-domain, intact BSE, L4 loop, stalk domain, and the mediated oligomerization were previously shown to be involved in its proper antiviral activity (54, 56–58). Here, in comparison, the N-terminal region (1–366 aa) mainly consisting of the G domain and two α-helix peptides of BSE is sufficient for MxA inhibition of DBV, indicating a different requirement of the MxA functional domains. Additionally, we found that MxA overexpression can significantly repress DBV RNP activity and the viral replication. However, despite the involvement of MxA in interference with IAV RNP, overexpression of MxA alone is insufficient to block IAV RNP nuclear import and other host proteins are

required (59, 60). Thus, our present findings likely suggest a new mode of action for MxA antiviral activities with characteristics and requirements distinct from those previously proposed, expanding the knowledge of not only the antiviral spectrum of MxA but also the underlying mechanisms.

As stated above, the N-terminal region of MxA is identified as the functional domain that restricted DBV infection to comparable extents with the full-length protein. Consistently, mechanistic analyses validated that, indeed, this head region alone can target to NP by acting as the binding domain and impair the NP-RdRp interaction. MxA C-terminal is required for its oligomer formation and oligomerization-dependent GTP hydrolysis (56, 57). Thus, the finding reflects that these related activities of MxA (including the oligomerization and GTP hydrolysis) are likely dispensable for inhibition of DBV. Subsequently, we further showed an important role of T103 in MxA anti-DBV activity, which is located in the N-terminal head region (61). Also consistent with the mechanism model, T103 is likely required for efficient binding of MxA to NP and the resultant obstruction of the NP-RdRp interaction. These analyses not only characterize the functional region for MxA anti-DBV activity but also further support the new antiviral mechanism model of MxA presented here. More other amino acids possibly involved in the N-terminal region-mediated anti-DBV activity remain to be fully screened and elucidated in the future. Of note, natural mutations of MxA at certain amino acids of the N-terminal have been reported in human population (62, 63). These mutations can lead to attenuation of the MxA anti-IAV activity and might contribute to greater susceptibility to IAV (63–65). Similarly, it might be merited to explore the potential effects of single-nucleotide polymorphisms of antiviral genes like MxA on the pathogenicity of DBV in the future.

Following the identification of DBV, several other novel viruses that are genetically related to DBV were successively discovered around the world (66–69). These viruses have been classified into the new *Bandavirus* genus according to the latest report by International Committee on Taxonomy of Viruses (ICTV) and posed an increasing threat to the global public health (49, 69). Particularly, Heartland virus that was first isolated from two Missouri patients and subsequently found to be widespread within the central and eastern United States can cause severe clinical manifestations and even deaths similar to SFTS (70). The NP proteins of HRTV and DBV share 62% identify (70). It is possible that MxA may act as a common restriction factor against the bandaviruses by the similar mechanism. Further validating and comparative studies on these viruses may provide general insights into the virus-host interactions which might help advance the development of broad-spectrum antiviral therapies against these emerging pathogens.

MATERIALS AND METHODS

Cells and virus infection

HEK293T (ATCC, CRL-11268), A549 (ATCC, CCL-185), Vero (ATCC, CCL-81), and BHK21 (ATCC, CCL-10) cells were cultured in Dulbecco's modified Eagle's medium (DMEM) supplemented with 10% fetal bovine serum (FBS) at 37˚C with 5% CO_2. HEK293 (ATCC, CRL-1573) and THP-1 (ATCC, TWB-202) cells were maintained in minimum Eagle's medium (MEM) and Roswell Park Memorial Institute (RPMI) 1640 medium supplemented with 10% FBS, respectively. MxA-KO HEK293 cells were generated via CRISPR-Cas9 gene editing, as described below. Dabie bandavirus, i.e., SFTS virus (SFTSV, strain WCH) was propagated and titrated using the 50% tissue culture infectious dose (TCID50) method as previously described (12, 16, 71).

Plasmids and transfection

The MxA and MxA mutant expression plasmids were constructed by cloning the open reading frame of MxA or mutants into the pcDNA3.1(+) vector, with an N-terminal Flag tag. The C-terminal fusion of MxA to a Stag was constructed by cloning in pCAGGSP7

vector (16). The EGFP-fused NP or N-arm expression plasmids were constructed using the pEGFP-N1 vector as previously described (12). The plasmids expressing DBV NP or RdRp and the minigenome reporter plasmids were previously described (36). Transfection was performed using the Lipofectamine 3000 transfection reagent (Thermo Fisher Scientific) by following the manufacturer's instructions.

Antibodies

The rabbit antisera to SFTVS NP, NSs, GP (Gn), or RdRp were prepared in house as previously described (12, 18). The following antibodies were purchased from the indicated manufacturers: rabbit anti-MxA polyclonal antibody (pAb) (Proteintech, Cat#13750–1-AP), mouse anti-Flag monoclonal antibody (mAb) (Sigma-Aldrich, Cat#F3165), rabbit anti-β-actin mAb (ABclonal, Cat#AC026), rabbit anti-Stag pAb (Abcam, Cat#ab18588), mouse anti-HA mAb (ABclonal, Cat#AE008), and rabbit anti-EGFP pAb (Abcam, Cat#ab6556). For the secondary antibodies, goat anti-mouse IgG conjugated with Alexa Fluor 488 (Thermo Fisher Scientific, Cat#A-11001) and goat anti-rabbit IgG conjugated with Alexa Fluor 647 (Thermo Fisher Scientific, Cat#A32733) were used in the IFA assay. In Western blot analysis, goat anti-mouse or anti-rabbit IgG antibodies conjugated with HRP (Abcam, Cat#ab6789 and Cat#ab6721) were used.

Protein interaction analysis

Protein interaction analyses were performed as previously described (12, 20, 72). Briefly, for S-pulldown assays, HEK293T cells were co-transfected with the S-tagged protein expression plasmids and other indicated plasmids and lysed 24 h post-transfection using Western blot/IP lysis buffer (Beyotime, Cat#P0013). The cell lysate supernatants were then incubated with S-protein agarose (Millipore, Cat#69704). After extensive washing of the agarose, binding proteins were eluted using 1 × sodium dodecyl sulfate (SDS) sample buffer, boiled, and analyzed using SDS-polyacrylamide gel electrophoresis (SDS-PAGE) and Western blot analysis. For nuclease treatment analysis (36), cell lysates supplemented with 5 mM $MgCl_2$ were divided into halves and then treated with UltraNuclease (Yeasen, Cat#20157ES25) or left untreated at 4°C for 4 h according to the manufacturer's instructions before S-pulldown assays. For the EGFP-nano trap assays, cells transfected with the indicated plasmids encoding EGFP or EGFP-fused proteins were lysed and clarified similarly. The lysate supernatants were then incubated with anti-GFP nanobody-coated agarose beads (AlpaLife, Cat#KTSM1301) that are covalently coupled with nanoantibodies to EGFP. After extensively washing, binding proteins were eluted and analyzed by Western blot. For the HA-pulldown assays, HEK293T cells were transfected with the indicated plasmids encoding HA-fused proteins and lysed similarly. The lysate supernatants were then incubated with anti-HA magnetic beads (MedChemExpress, Cat#HY-K0201). The beads were washed three times and eluted with 1 × SDS loading buffer, followed by Western blot analysis.

Western blot analysis

Protein samples were subjected to SDS-PAGE and then transferred to polyvinylidene difluoride (PVDF) membranes (Millipore, Cat#L3000015). After incubation with 5% skimmed milk in Tris-buffered saline, the PVDF membranes were treated with primary antibodies and then with corresponding horseradish peroxidase (HRP)-conjugated secondary antibodies. Detection was carried out using a chemiluminescence kit (Thermo Fisher Scientific, Cat#34580) and analyzed quantitatively using ImageJ software (National Institutes of Health).

Immunofluorescence and confocal microscopy

HeLa cells mock-infected or infected with DBV were washed with PBS, fixed with 4% paraformaldehyde in phosphate-buffered saline (PBS) for 10 min at room temperature, permeabilized with 0.1% Triton X-100 in PBS for 15 min, and blocked with 5% BSA in

TABLE 1 Oligonucleotides used in this study

Name	Sequence (5′–3′)	Purpose
sgMxA	AAGATGGTTGTTTCCGAAG	sgRNA target sequence for *MxA*-KO
qGAPDH-F	CATCACCATCTTCCAGGAGCGAGA	GAPDH, qPCR forward primer
qGAPDH-R	TGCAGGAGGCATTGCTGATGATCT	GAPDH, qPCR reverse primer
qMxA-F	CTACACACCGTGACGGATATG	MxA, qPCR forward primer
qMxA-R	CGAGCTGGATTGGAAAGCCC	MxA, qPCR reverse primer
qDBV-S-F	CTGGGCAATGGAAACCGGAAG	S RNA, qPCR forward primer
qDBV-S-R	CAATGAGGAAGAAGTGAACAAGT	S RNA, qPCR reverse primer
qDBV-M-F	TGTGGAGGGATGCGTGTCAGA	M RNA, qPCR reverse primer
qDBV-M-R	AGTGGAATTGAATCTCCGTGCT	M RNA, qPCR reverse primer
qDBV-L-F	TCACGCCACTGCTTTCGCTTT	L RNA, qPCR forward primer
qDBV-L-R	CGGCTCCTGACAATGTTCCT	L RNA, qPCR reverse primer

PBS for 30 min. The cells were then incubated with rabbit anti-NP (1:1,000) and mouse anti-Flag (1:1,000) primary antibodies in 5% BSA overnight at 4°C and stained with fluorescein-labeled secondary antibodies for 2 h at room temperature. To visualize the nuclei, cells were stained with Hoechst 33258 (Beyotime, Cat#C1011) for 5 min at room temperature. Images were captured using an ANDOR confocal microscope (UltraVIEW VoX) and analyzed using ImageJ software.

Generation of the MxA-KO cells line by CRISPR-Cas9

The guide RNA (gRNA) sequence was selected using the online CRISPR Design tool (http://crispr.mit.edu/) and cloned into pX459 (Table 1) (12, 73). HEK293 cells were transfected with the constructed pX459-based plasmids and selected with 2 µg/mL puromycin (Beyotime, Cat#ST551-10 mg) for 48 h. The cells were then diluted and seeded into 96-well plates for single colony screening by Western blot and sequencing. The regions encompassing the gRNA-targeted sequences were amplified and purified for sequencing analysis of the editing site.

Virus growth curve analysis

HEK293 cells with MxA KO or overexpression, or control cells, were incubated with DBV (0.1 MOI) at 37°C for 2 h. After three washes, the cells were incubated at 37°C for the indicated time. The cell culture supernatants collected at the indicated time points were subjected to viral titration by TCID50 assays using Vero cells as previously described (16, 18, 74, 75).

Minigenome reporter assay

Minigenome reporter assay for RNP activity was performed as described previously (36). BHK21 cells seeded in 96-well plates were co-transfected with the DBV RdRp (50 ng/well) and NP (25 ng/well) expression plasmids, and the PolI-MUTR-EGFP transcription plasmid (25 ng/well), together with the plasmid expressing Flag-MxA (50 ng/well) or control vector as indicated. The total amounts of plasmids transfected in each well were kept constant by the addition of control plasmids. At 48 h post-transfection, cells were stained with Hoechst 33258 (Beyotime, Cat#C1011) for 5 min at room temperature, followed by an analysis of total and EGFP-positive cell counts using the Operetta CLSTM high-throughput system (PerkinElmer). EGFP-positive cell proportion was calculated and normalized to the RNP reconstitution control group without Flag-MxA expression. A similar minigenome assay with firefly luciferase (Fluc) as the reporter was also conducted, confirming the conclusion. In the system, a PolI-MUTR-Fluc transcription plasmid (20 ng/well) and an internal control pRL-TK (5 ng/well) expressing *Renilla* luciferase (Rluc) were used for co-transfection to replace the PolI-MUTR-EGFP transcription plasmid, followed

by dual luciferase reporter detection (36). Relative luciferase activities were calculated by normalization to the Rluc activities (16).

Virus binding and internalization assays

HEK293T cells transfected with the indicated expression plasmids were incubated with DBV (50 MOI) on ice for 1 h for virus binding. The cells were then washed three times with ice-cold PBS to remove the unbound viruses, followed by RNA extraction and qPCR analysis of the bound viruses. Alternatively, to detect the internalized virus, the bound virus-cell mixture was further transferred to 37°C for 30 min. Subsequently, the samples were washed once with PBS and treated with 500 ng/mL proteinase K on ice for 1 h to remove un-internalized viruses. After three cycles of washings, the internalized viruses were then quantified by qPCR analysis.

Chemical cross-linking

Chemical cross-linking analysis of N oligomerization was conducted as previously described (12, 42). HEK293 cells were transfected with either the control vector or the plasmids expressing Flag-MxA, along with the DBV NP expression plasmid. At 48 h post-transfection, cells were digested by 0.5% trypsin, washed and suspended with PBS, and incubated with the crosslinker disuccinimidyl suberate (DSS, 5 mM; Thermo Fisher Scientific, Cat#A39267) in PBS at room temperature for 30 min. Then, the reaction was stopped by 20 mM Tris (pH 7.5) at room temperature for 15 min, followed by SDS-PAGE resolution and Western blot analysis.

Real-time qPCR

Total RNAs was extracted from cells using TRIzol (Takara, Cat#15596018), followed by reverse transcription to cDNA using Prime Script RT regent Kit with gDNA Eraser (TaKaRa, Cat#RR047). Reverse transcribed cDNA was used as the template in quantitative PCR with TB Green Premix Ex Taq II (TaKaRa, Cat#RR820). The qPCR reactions were run on an ABI StepOnePlus (Applied Biosystems). Relative RNA levels were quantified using the $2^{-\Delta\Delta CT}$ method by normalization to the mRNA levels of human GAPDH as described previously (19, 76). Primers used were listed in Table 1.

Quantification and statistical analysis

Graphs were generated by GraphPad Prism (version 8, GraphPad Software). All data are presented as means ± SD of *n* biological replicates. Statistical analyses were performed using Student's *t*-test for the comparison between two groups and one-way analysis of variance (ANOVA) for multiple comparisons. Differences were considered statistically significant if the *P*-value was less than 0.05. Significance levels are denoted as follows: *$P < 0.05$; **$P < 0.01$; ***$P < 0.001$; ****$P < 0.0001$; ns, non-significant.

ACKNOWLEDGMENTS

We thank the Core Facility and Technical Support of Wuhan Institute of Virology and the running team of National Biosafety Laboratory, Wuhan, Chinese Academy of Sciences for technical assistants. We would also like to thank Mrs. Min Zhou in National Virus Resource Center, Wuhan Institute of Virology, Chinese Academy of Sciences, for assisting the cell culture, and Mrs. Qiaoli Wu and Shuang Tang in National Virus Resource Center for providing technical support to virus preservation and subculture.

This work was supported by the National Key Research and Development Program of China (2022YFC2303300, to Y.J.N. and H.L.W.), the National Natural Science Foundation of China (32170171, to Y.J.N.), and the Youth Innovation Promotion Association of Chinese Academy of Sciences (to Y.J.N.).

H.L.W. and Y.J.N. supervised the research. Y.J.N. conceived the study. Y.J.N. and M.C. designed the experiments. M.C. performed the majority of the experiments and acquired

the data. Z.X. provided assistance in experiments during the revision. M.C. and Y.J.N. analyzed the data and prepared the figures. Y.J.N., Y.Q.M., and M.C. wrote the original draft. Y.J.N. reviewed and edited the manuscript. Y.J.N. and H.L.W. secured funding for the study. Y.J.N., F.D., and H.L.W. provided resources and experimental materials. All authors reviewed and approved the manuscript.

AUTHOR AFFILIATIONS

[1]Key Laboratory of Virology and Biosafety and National Virus Resource Center, Wuhan Institute of Virology, Chinese Academy of Sciences, Wuhan, China
[2]University of Chinese Academy of Sciences, Beijing, China
[3]State Key Laboratory of Virology and Center for Biosafety Mega-Science, Chinese Academy of Sciences, Wuhan, China
[4]Hubei Jiangxia Laboratory, Wuhan, China

AUTHOR ORCIDs

Fei Deng http://orcid.org/0000-0002-5385-083X
Hualin Wang http://orcid.org/0000-0001-8916-4578
Yun-Jia Ning http://orcid.org/0000-0001-7738-1524

FUNDING

Funder	Grant(s)	Author(s)
MOST | National Key Research and Development Program of China (NKPs)	2022YFC2303300	Hualin Wang Yun-Jia Ning
MOST | National Natural Science Foundation of China (NSFC)	32170171	Yun-Jia Ning
Youth Innovation Promotion Association of the Chinese Academy of Sciences (CAS YIPA)		Yun-Jia Ning

AUTHOR CONTRIBUTIONS

Meng Chang, Data curation, Formal analysis, Investigation, Methodology, Validation, Visualization, Writing – original draft | Yuan-Qin Min, Methodology, Resources, Visualization, Writing – original draft | Zhao Xu, Investigation | Fei Deng, Project administration, Resources | Hualin Wang, Funding acquisition, Project administration, Resources, Software, Supervision, Visualization | Yun-Jia Ning, Conceptualization, Funding acquisition, Methodology, Project administration, Resources, Supervision, Visualization, Writing – original draft, Writing – review and editing

REFERENCES

1. Yu X-J, Liang M-F, Zhang S-Y, Liu Y, Li J-D, Sun Y-L, Zhang L, Zhang Q-F, Popov VL, Li C, et al. 2011. Fever with thrombocytopenia associated with a novel bunyavirus in china. N Engl J Med 364:1523–1532. https://doi.org/10.1056/NEJMoa1010095
2. Zhang Y-Z, He Y-W, Dai Y-A, Xiong Y, Zheng H, Zhou D-J, Li J, Sun Q, Luo X-L, Cheng Y-L, et al. 2012. Hemorrhagic fever caused by a novel bunyavirus in China: pathogenesis and correlates of fatal outcome. Clin Infect Dis 54:527–533. https://doi.org/10.1093/cid/cir804
3. Kim K-H, Yi J, Kim G, Choi SJ, Jun KI, Kim N-H, Choe PG, Kim N-J, Lee J-K, Oh M. 2013. Severe fever with thrombocytopenia syndrome, South Korea, 2012. Emerg Infect Dis 19:1892–1894. https://doi.org/10.3201/eid1911.130792
4. Takahashi T, Maeda K, Suzuki T, Ishido A, Shigeoka T, Tominaga T, Kamei T, Honda M, Ninomiya D, Sakai T, et al. 2014. The first identification and retrospective study of severe fever with thrombocytopenia syndrome in Japan. J Infect Dis 209:816–827. https://doi.org/10.1093/infdis/jit603
5. Hu B, Cai K, Liu M, Li W, Xu J, Qiu F, Zhan J. 2018. Laboratory detection and molecular phylogenetic analysis of severe fever with thrombocytopenia syndrome virus in Hubei province, central China. Arch Virol 163:3243–3254. https://doi.org/10.1007/s00705-018-3993-5
6. Tran XC, Yun Y, Van An L, Kim S-H, Thao NTP, Man PKC, Yoo JR, Heo ST, Cho N-H, Lee KH. 2019. Endemic severe fever with thrombocytopenia syndrome, Vietnam. Emerg Infect Dis 25:1029–1031. https://doi.org/10.3201/eid2505.181463
7. Word Health Organization (WHO). 2017. Annual review of diseases prioritized under the research and development blueprint. Available from: http://www.who.int/csr/research-and-development/en/
8. Schmaljohn CS, Nichol ST. 2007. Bunyaviridae, p 1741–1789. In Knipe DM, PM Howley (ed), Fields virology, 5th edn. Lippincott, Williams & Wilkins.
9. Taxonomy of the order Bunyavirales: version 3 of MSL38, the 2022 ICTV taxonomy. https://ictv.global/news/taxonomy-2022.3.
10. Sun Y, Li J, Gao GF, Tien P, Liu W. 2018. Bunyavirales ribonucleoproteins: the viral replication and transcription machinery. Crit Rev Microbiol 44:522–540. https://doi.org/10.1080/1040841X.2018.1446901

11. Malet H, Williams HM, Cusack S, Rosenthal M. 2023. The mechanism of genome replication and transcription in bunyaviruses. PLoS Pathog 19:e1011060. https://doi.org/10.1371/journal.ppat.1011060
12. Mo Q, Xu Z, Deng F, Wang H, Ning Y-J. 2020. Host restriction of emerging high-pathogenic bunyaviruses via MOV10 by targeting viral nucleoprotein and blocking ribonucleoprotein assembly. PLoS Pathog 16:e1009129. https://doi.org/10.1371/journal.ppat.1009129
13. Cheng E, Wang Z, Mir MA. 2014. Interaction between hantavirus nucleocapsid protein (N) and RNA-dependent RNA polymerase (RdRp) mutants reveals the requirement of an N-RdRp interaction for viral RNA synthesis. J Virol 88:8706–8712. https://doi.org/10.1128/JVI.00405-14
14. Tani H, Shimojima M, Fukushi S, Yoshikawa T, Fukuma A, Taniguchi S, Morikawa S, Saijo M. 2016. Characterization of glycoprotein-mediated entry of severe fever with thrombocytopenia syndrome virus. J Virol 90:5292–5301. https://doi.org/10.1128/JVI.00110-16
15. Yuan F, Zheng A. 2017. Entry of severe fever with thrombocytopenia syndrome virus. Virol Sin 32:44–50. https://doi.org/10.1007/s12250-016-3858-6
16. Ning YJ, Wang M, Deng M, Shen S, Liu W, Cao WC, Deng F, Wang YY, Hu Z, Wang H. 2014. Viral suppression of innate immunity via spatial isolation of TBK1/IKKepsilon from mitochondrial antiviral platform. J Mol Cell Biol 6:324–337. https://doi.org/10.1093/jmcb/mju015
17. Ning YJ, Feng K, Min YQ, Cao WC, Wang M, Deng F, Hu Z, Wang H. 2015. Disruption of type I interferon signaling by the nonstructural protein of severe fever with thrombocytopenia syndrome virus via the hijacking of STAT2 and STAT1 into inclusion bodies. J Virol 89:4227–4236. https://doi.org/10.1128/JVI.00154-15
18. Ning Y-J, Mo Q, Feng K, Min Y-Q, Li M, Hou D, Peng C, Zheng X, Deng F, Hu Z, Wang H. 2019. Interferon-γ-directed inhibition of a novel high-pathogenic phlebovirus and viral antagonism of the antiviral signaling by targeting STAT1. Front Immunol 10:1182. https://doi.org/10.3389/fimmu.2019.01182
19. Min Y-Q, Ning Y-J, Wang H, Deng F. 2020. A RIG-I-like receptor directs antiviral responses to a bunyavirus and is antagonized by virus-induced blockade of TRIM25-mediated ubiquitination. J Biol Chem 295:9691–9711. https://doi.org/10.1074/jbc.RA120.013973
20. Feng K, Zhang H, Jiang Z, Zhou M, Min YQ, Deng F, Li P, Wang H, Ning YJ. 2023. SFTS bunyavirus NSs protein sequestrates mTOR into inclusion bodies and deregulates mTOR-ULK1 signaling, provoking pro-viral autophagy. J Med Virol 95. https://doi.org/10.1002/jmv.28371
21. Gao C, Yu Y, Wen C, Li Z, Ding H, Qi X, Cardona CJ, Xing Z. 2022. Nonstructural protein NSs activates inflammasome and pyroptosis through interaction with NLRP3 in human microglial cells infected with severe fever with thrombocytopenia syndrome bandavirus. J Virol 96:e0016722. https://doi.org/10.1128/jvi.00167-22
22. Yoshikawa R, Sakabe S, Urata S, Yasuda J. 2019. Species-specific pathogenicity of severe fever with thrombocytopenia syndrome virus is determined by anti-STAT2 activity of NSs. J Virol 93:e02226-18. https://doi.org/10.1128/JVI.02226-18
23. Liu H, Liu S, Liu Z, Gao X, Xu L, Huang M, Su Y, Wang Z, Wang T. 2022. Dabie bandavirus nonstructural protein interacts with actin to induce F-actin rearrangement and inhibit viral adsorption and entry. J Virol 96:e0078822. https://doi.org/10.1128/jvi.00788-22
24. Santiago FW, Covaleda LM, Sanchez-Aparicio MT, Silvas JA, Diaz-Vizarreta AC, Patel JR, Popov V, Yu X, García-Sastre A, Aguilar PV, Williams B. 2014. Hijacking of RIG-I signaling proteins into virus-induced cytoplasmic structures correlates with the inhibition of type I interferon responses. J Virol 88:4572–4585. https://doi.org/10.1128/JVI.03021-13
25. Wu X, Qi X, Qu B, Zhang Z, Liang M, Li C, Cardona CJ, Li D, Xing Z, Ross SR. 2014. Evasion of antiviral immunity through sequestering of TBK1/IKKε/IRF3 into viral inclusion bodies. J Virol 88:3067–3076. https://doi.org/10.1128/JVI.03510-13
26. Yamada S, Shimojima M, Narita R, Tsukamoto Y, Kato H, Saijo M, Fujita T. 2018. RIG-I-like receptor and toll-like receptor signaling pathways cause aberrant production of inflammatory cytokines/chemokines in a severe fever with thrombocytopenia syndrome virus infection mouse model. J Virol 92:e02246-17. https://doi.org/10.1128/JVI.02246-17
27. Schneider WM, Chevillotte MD, Rice CM. 2014. Interferon-stimulated genes: a complex web of host defenses. Annu Rev Immunol 32:513–545. https://doi.org/10.1146/annurev-immunol-032713-120231
28. Pavlovic J, Arzet HA, Hefti HP, Frese M, Rost D, Ernst B, Kolb E, Staeheli P, Haller O. 1995. Enhanced virus resistance of transgenic mice expressing the human MxA protein. J Virol 69:4506–4510. https://doi.org/10.1128/JVI.69.7.4506-4510.1995
29. Frese M, Kochs G, Feldmann H, Hertkorn C, Haller O. 1996. Inhibition of bunyaviruses, phleboviruses, and hantaviruses by human MxA protein. J Virol 70:915–923. https://doi.org/10.1128/JVI.70.2.915-923.1996
30. Hefti HP, Frese M, Landis H, Di Paolo C, Aguzzi A, Haller O, Pavlovic J. 1999. Human MxA protein protects mice lacking a functional alpha/beta interferon system against La crosse virus and other lethal viral infections. J Virol 73:6984–6991. https://doi.org/10.1128/JVI.73.8.6984-6991.1999
31. Mundt E. 2007. Human MxA protein confers resistance to double-stranded RNA viruses of two virus families. J Gen Virol 88:1319–1323. https://doi.org/10.1099/vir.0.82526-0
32. Dittmann J, Stertz S, Grimm D, Steel J, García-Sastre A, Haller O, Kochs G. 2008. Influenza A virus strains differ in sensitivity to the antiviral action of Mx-GTPase. J Virol 82:3624–3631. https://doi.org/10.1128/JVI.01753-07
33. Netherton CL, Simpson J, Haller O, Wileman TE, Takamatsu HH, Monaghan P, Taylor G. 2009. Inhibition of a large double-stranded DNA virus by MxA protein. J Virol 83:2310–2320. https://doi.org/10.1128/JVI.00781-08
34. Verhelst J, Hulpiau P, Saelens X. 2013. Mx proteins: antiviral gatekeepers that restrain the uninvited. Microbiol Mol Biol Rev 77:551–566. https://doi.org/10.1128/MMBR.00024-13
35. Zhou H, Sun Y, Wang Y, Liu M, Liu C, Wang W, Liu X, Li L, Deng F, Wang H, Guo Y, Lou Z. 2013. The nucleoprotein of severe fever with thrombocytopenia syndrome virus processes a stable hexameric ring to facilitate RNA encapsidation. Protein Cell 4:445–455. https://doi.org/10.1007/s13238-013-3901-4
36. Ren F, Shen S, Ning Y-J, Wang Q, Dai S, Shi J, Zhou M, Wang H, Huang C, Zhang D-Y, Deng F. 2021. Non-structural proteins of severe fever with thrombocytopenia syndrome virus suppress RNA synthesis in a transcriptionally active cDNA-derived viral RNA synthesis system. Front Microbiol 12:709517. https://doi.org/10.3389/fmicb.2021.709517
37. Zhang R, Kim AS, Fox JM, Nair S, Basore K, Klimstra WB, Rimkunas R, Fong RH, Lin H, Poddar S, Crowe JE, Doranz BJ, Fremont DH, Diamond MS. 2018. Mxra8 is a receptor for multiple arthritogenic alphaviruses. Nature 557:570–574. https://doi.org/10.1038/s41586-018-0121-3
38. Zhao X, Zhang G, Liu S, Chen X, Peng R, Dai L, Qu X, Li S, Song H, Gao Z, et al. 2019. Human neonatal Fc receptor is the cellular uncoating receptor for enterovirus B. Cell 177:1553–1565. https://doi.org/10.1016/j.cell.2019.04.035
39. Li M, Liu C, Xu X, Liu Y, Jiang Z, Li Y, Lv Y, Lu S, Hu C, Mao H. 2020. Grass carp (*Ctenopharyngodon idella*) GPATCH3 initiates IFN 1 expression via the activation of STING-IRF7 signal axis. Dev Comp Immunol 112:103781. https://doi.org/10.1016/j.dci.2020.103781
40. Lv Y, Deng H, Liu Y, Chang K, Du H, Zhou P, Mao H, Hu C. 2021. The tyrosine kinase SRC of grass carp (*Ctenopharyngodon idellus*) up-regulates the expression of IFN I by activating TANK binding kinase 1. Dev Comp Immunol 114:103834. https://doi.org/10.1016/j.dci.2020.103834
41. Li B, Wang Q, Pan X, Fernández de Castro I, Sun Y, Guo Y, Tao X, Risco C, Sui S-F, Lou Z. 2013. Bunyamwera virus possesses a distinct nucleocapsid protein to facilitate genome encapsidation. Proc Natl Acad Sci U S A 110:9048–9053. https://doi.org/10.1073/pnas.1222552110
42. Alfadhli A, Love Z, Arvidson B, Seeds J, Willey J, Barklis E. 2001. Hantavirus nucleocapsid protein oligomerization. J Virol 75:2019–2023. https://doi.org/10.1128/JVI.75.4.2019-2023.2001
43. Li N, Zhang L, Chen L, Feng W, Xu Y, Chen F, Liu X, Chen Z, Liu W. 2012. MxA inhibits hepatitis B virus replication by interaction with hepatitis B core antigen. Hepatology 56:803–811. https://doi.org/10.1002/hep.25608
44. Patzina C, Haller O, Kochs G. 2014. Structural requirements for the antiviral activity of the human MxA protein against thogoto and influenza A virus. J Biol Chem 289:6020–6027. https://doi.org/10.1074/jbc.M113.543892
45. Reichelt M, Stertz S, Krijnse-Locker J, Haller O, Kochs G. 2004. Missorting of lacrosse virus nucleocapsid protein by the interferon-induced MxA GTPase involves smooth ER membranes. Traffic 5:772–784. https://doi.org/10.1111/j.1600-0854.2004.00219.x

46. Nigg PE, Pavlovic J. 2015. Oligomerization and GTP-binding requirements of MxA for viral target recognition and antiviral activity against influenza A virus. J Biol Chem 290:29893–29906. https://doi.org/10.1074/jbc.M115.681494
47. Kochs G, Haller O. 1999. GTP-bound human MxA protein interacts with the nucleocapsids of thogoto virus (orthomyxoviridae). J Biol Chem 274:4370–4376. https://doi.org/10.1074/jbc.274.7.4370
48. Yu Z, Wang Z, Chen J, Li H, Lin Z, Zhang F, Zhou Y, Hou J. 2008. GTPase activity is not essential for the interferon-inducible MxA protein to inhibit the replication of hepatitis B virus. Arch Virol 153:1677–1684. https://doi.org/10.1007/s00705-008-0168-9
49. Paules CI, Marston HD, Bloom ME, Fauci AS. 2018. Tickborne diseases - confronting a growing threat. N Engl J Med 379:701–703. https://doi.org/10.1056/NEJMp1807870
50. Hornak KE, Lanchy J-M, Lodmell JS. 2016. RNA encapsidation and packaging in the phleboviruses. Viruses 8:194. https://doi.org/10.3390/v8070194
51. Zürcher T, Pavlovic J, Staeheli P. 1992. Mechanism of human MxA protein action: variants with changed antiviral properties. EMBO J 11:1657–1661. https://doi.org/10.1002/j.1460-2075.1992.tb05212.x
52. Kochs G, Haller O. 1999. Interferon-induced human MxA GTPase blocks nuclear import of thogoto virus nucleocapsids. Proc Natl Acad Sci U S A 96:2082–2086. https://doi.org/10.1073/pnas.96.5.2082
53. Verhelst J, Van Hoecke L, Spitaels J, De Vlieger D, Kolpe A, Saelens X. 2017. Chemical-controlled activation of antiviral myxovirus resistance protein 1. J Biol Chem 292:2226–2236. https://doi.org/10.1074/jbc.M116.748806
54. Haller O, Staeheli P, Schwemmle M, Kochs G. 2015. Mx GTPases: dynamin-like antiviral machines of innate immunity. Trends Microbiol 23:154–163. https://doi.org/10.1016/j.tim.2014.12.003
55. Schattgen SA, Oguin TH, Thomas PG. 2016. The antiviral molecule Mx1 positively regulates the induction of type I IFN in response to influenza infection. J Immunol Res 196:202. https://doi.org/10.4049/jimmunol.196.Supp.202.7
56. Gao S, von der Malsburg A, Paeschke S, Behlke J, Haller O, Kochs G, Daumke O. 2010. Structural basis of oligomerization in the stalk region of dynamin-like MxA. Nature 465:502–506. https://doi.org/10.1038/nature08972
57. Gao S, von der Malsburg A, Dick A, Faelber K, Schröder GF, Haller O, Kochs G, Daumke O. 2011. Structure of myxovirus resistance protein a reveals intra- and intermolecular domain interactions required for the antiviral function. Immunity 35:514–525. https://doi.org/10.1016/j.immuni.2011.07.012
58. Jimah JR, Hinshaw JE. 2019. Structural insights into the mechanism of dynamin superfamily proteins. Trends Cell Biol 29:257–273. https://doi.org/10.1016/j.tcb.2018.11.003
59. Long JS, Mistry B, Haslam SM, Barclay WS. 2019. Host and viral determinants of influenza A virus species specificity. Nat Rev Microbiol 17:67–81. https://doi.org/10.1038/s41579-018-0140-y
60. Zimmermann P, Mänz B, Haller O, Schwemmle M, Kochs G. 2011. The viral nucleoprotein determines Mx sensitivity of influenza A viruses. J Virol 85:8133–8140. https://doi.org/10.1128/JVI.00712-11
61. Haller O, Kochs G. 2002. Interferon-induced Mx proteins: dynamin-like GTPases with antiviral activity. Traffic 3:710–717. https://doi.org/10.1034/j.1600-0854.2002.31003.x
62. Graf L, Dick A, Sendker F, Barth E, Marz M, Daumke O, Kochs G. 2018. Effects of allelic variations in the human myxovirus resistance protein A on its antiviral activity. J Biol Chem 293:3056–3072. https://doi.org/10.1074/jbc.M117.812784
63. Chen Y, Graf L, Chen T, Liao Q, Bai T, Petric PP, Zhu W, Yang L, Dong J, Lu J, Chen Y, Shen J, Haller O, Staeheli P, Kochs G, Wang D, Schwemmle M, Shu Y. 2021. Rare variant Mx1 alleles increase human susceptibility to zoonotic H7N9 influenza virus. Science 373:918–922. https://doi.org/10.1126/science.abg5953
64. Haller O, Kochs G. 2020. Mx genes: host determinants controlling influenza virus infection and trans-species transmission. Hum Genet 139:695–705. https://doi.org/10.1007/s00439-019-02092-8
65. Petric PP, King J, Graf L, Pohlmann A, Beer M, Schwemmle M. 2022. Increased polymerase activity of zoonotic H7N9 allows partial escape from MxA. Viruses 14:2331. https://doi.org/10.3390/v14112331
66. Mourya DT, Yadav PD, Basu A, Shete A, Patil DY, Zawar D, Majumdar TD, Kokate P, Sarkale P, Raut CG, Jadhav SM. 2014. Malsoor virus, a novel bat phlebovirus, is closely related to severe fever with thrombocytopenia syndrome virus and heartland virus. J Virol 88:3605–3609. https://doi.org/10.1128/JVI.02617-13
67. Wang J, Selleck P, Yu M, Ha W, Rootes C, Gales R, Wise T, Crameri S, Chen H, Broz I, Hyatt A, Woods R, Meehan B, McCullough S, Wang LF. 2014. Novel phlebovirus with zoonotic potential isolated from ticks, Australia. Emerg Infect Dis 20:1040–1043. https://doi.org/10.3201/eid2006.140003
68. Kohl C, Brinkmann A, Radonić A, Dabrowski PW, Nitsche A, Mühldorfer K, Wibbelt G, Kurth A. 2020. Zwiesel bat banyangvirus, a potentially zoonotic huaiyangshan banyangvirus (formerly known as SFTS)-like banyangvirus in northern bats from Germany. Sci Rep 10:1370. https://doi.org/10.1038/s41598-020-58466-w
69. Kuhn JH, Adkins S, Alkhovsky SV, Avšič-Županc T, Ayllón MA, Bahl J, Balkema-Buschmann A, Ballinger MJ, Bandte M, Beer M, et al. 2022. 2022 taxonomic update of phylum negarnaviricota (riboviria: orthornavirae), including the large orders bunyavirales and mononegavirales. Arch Virol 167:2857–2906.
70. McMullan LK, Folk SM, Kelly AJ, MacNeil A, Goldsmith CS, Metcalfe MG, Batten BC, Albariño CG, Zaki SR, Rollin PE, Nicholson WL, Nichol ST. 2012. A new phlebovirus associated with severe febrile illness in missouri. N Engl J Med 367:834–841. https://doi.org/10.1056/NEJMoa1203378
71. Feng K, Deng F, Hu Z, Wang H, Ning YJ. 2019. Heartland virus antagonizes type I and III interferon antiviral signaling by inhibiting phosphorylation and nuclear translocation of STAT2 and STAT1. J Biol Chem 294:9503–9517. https://doi.org/10.1074/jbc.RA118.006563
72. Feng K, Zhang H-J, Min Y-Q, Zhou M, Deng F, Wang H-L, Li P-Q, Ning Y-J. 2023. SARS-CoV-2 NSP13 interacts with host IRF3, blocking antiviral immune responses. J Med Virol 95:e28881. https://doi.org/10.1002/jmv.28881
73. Ran FA, Hsu PD, Wright J, Agarwala V, Scott DA, Zhang F. 2013. Genome engineering using the CRISPR-Cas9 system. Nat Protoc 8:2281–2308. https://doi.org/10.1038/nprot.2013.143
74. Ning YJ, Feng K, Min YQ, Deng F, Hu Z, Wang H. 2017. Heartland virus NSs protein disrupts host defenses by blocking the TBK1 kinase-IRF3 transcription factor interaction and signaling required for interferon induction. J Biol Chem 292:16722–16733. https://doi.org/10.1074/jbc.M117.805127
75. Lei C, Yang J, Hu J, Sun X. 2021. On the calculation of TCID(50) for quantitation of virus infectivity. Virol Sin 36:141–144. https://doi.org/10.1007/s12250-020-00230-5
76. Livak KJ, Schmittgen TD. 2001. Analysis of relative gene expression data using real-time quantitative PCR and the 2(-Delta Delta C(T)) method. Methods 25:402–408. https://doi.org/10.1006/meth.2001.1262